LEIDEN UNIVERSITY

Study of BCG-Substracted Images of Nearby Clusters

by

Juan Manuel Espejo Salcedo

Advisor:

Dr. Henk Hoekstra

Natural Sciences Faculty
Sterrenwacht

May 2017

"Not only is the Universe stranger than we think, it is stranger than we can think.."

Werner Heisenberg

Abstract

Natural Sciences Faculty

Sterrenwacht

We have obtained deep imaging data for a sample of low redshift massive clusters. The light from the BGC overwhelms the images from background galaxies and faint cluster members in the cluster core, and needs to be carefully subtracted. This is expected to reveal background galaxies that are strongly lensed. Identifying such systems allows for unique follow-up studies. Also the number density of faint cluster members may tell us something about the dynamical state of the cluster and how BGCs form. The aim of this project is to model the BCG light and search for strong lensing candidates and study the properties of faint cluster members in the core..

Acknowledgements

I would like to thank ...

Contents

List of Figures

Dedicated to my parents, whose love and support are my biggest motivation. . .

Chapter 1

Introduction

The history of the formation of stars is a key topic in the understanding of galaxies since it determines most of the physical processes of the initial stages and evolution of these building blocks of our Universe. Understanding the way stars form allows us to comprehend many physical properties of their host galaxies thus providing a useful framework on which to build a more elaborate theory of their subsequent evolution. We might have good ideas and some general agreement in the basics of formation of stars in galaxies, but our observational limitations don't allow us to say much about distant objects which we need to make a more elaborate and complete theory. In principle, we can't assume that all the stars have the same formation history in every galaxy and for every epoch of the Universe. The gas clouds that form stars might or might not create the same mixture of stars in every stellar system so it is important to see under what conditions we could assume a general trend and what implications in our observations this may have.

For galaxies that are far away, it is impossible to make star counts with our current technology, for this reason, their mass-to-light-ratio Υ (given by their stellar populations) provides a simple constraint on their initial mass function (IMF, which is a very fundamental and important quantity in the study of stellar systems because it constraints the physics of star formation but also because it allows us to infer stellar masses through observed luminosities.) as discussed by Russell J. Smith & John R. Lucey, 2013. Everything we know from galaxy evolution is implicitly assuming an explicit form of the IMF, with very little variations since it is the method we use to connect evolutionary sequences, this of course, given the fact that if every galaxy had its own IMF then it would be too difficult to study their evolution because of the lack of any knowledge about their history. We have some observational information about IMF in galaxies, in the case of spiral galaxies for example, the most commonly used IMFs are Chabrier or

Kroupa which are decently constrained given the facilities of our observations in our own galaxy. Also, bulges appear to have heavier IMFs than disks as mentioned by (Brewer et. al 2012), but our current understanding of this topic is still quite far from being satisfactory.

Although these naive assumptions given by our limited observational evidence might not be too far from reality, we must note that when we study more complex and dense systems like the brightest cluster galaxies (BCG) in galaxy clusters or giant elliptical galaxies in general, constraining the IMF via $M_\star/L$ might be way more complex and poses a greater challenge since masses are more difficult to establish for dynamically-hot systems like them. Measuring Υ in these systems is not a truly accurate constraint on the IMF since we may have different stellar formation histories than the ones associated with galaxies that are being formed now. These objects have a very old origin (although their build up and morphological formation is recent) because their stellar populations are old and they correspond to the highest density peak, so it is difficult to relate their stellar populations accurately.

This general view shows that in the context of the evolution of galaxies, there are many things that come together at the very heart of cosmology but also in the context of the stellar astrophysics and they need to be consistent with each other. Addressing this problem is complex for many reasons, one of them is that these systems have a strong dependency on their non-baryonic matter content which affects the mass-to-light-ratio determination. This dark matter contribution accounts for most of the dynamical mass of galaxies and it's the dominant contribution in most of their spacial scales, specially in the outter regions. The problem would be much easier to study if we only had the stellar mass because the light measurements would be enough to constrain the stellar populations, their evolution and their mass distribution.

Being able to calculate the percentage of dark matter allow us to define the IMF more precisely. So we want to see what fraction of the surface density is given by stars and what are the spatial scales in which DM becomes the dominant contribution to the enclosed mass. DM halos seem to have a diluted profile in comparison to the stellar content of galaxies (Navarro Frenk White, 1996) so there is a region near the center of these massive systems in which the stellar mass is the dominant contribution. This implies that accurate measurements of their luminosity could give precise determinations of their mass to light ratio thus giving us some knowledge of their IMFs.

Various techniques have been developed to try to understand the stellar populations that form these massive systems. One of them is by using gravitational lensing (Treu et. al. 2010) of background galaxies. Modelling the lensing configuration on a BCG provides a useful method to determine stellar and dark matter mass contribution in

elliptical galaxies, since it is difficult to constraint the IMF via $M_\star/L$ as mentioned before. Finding strong lensing in these systems can also give us information about the location of the mass center of the cluster through the lensing they produce. We usually assume that the centre of galaxy clusters lies in the BCGs (George et. al. 2012) but the real position of the centre in galaxy clusters is still an unsolved problem (Harvey et. al, 2017).

In this project we work with galaxy clusters that might be in the right range to search for gravitational lensing in the inner regions. We use deep data from CFHT that allows us to search for interesting targets and probe the relevant spacial scales. We focus on the brightest cluster galaxy since it is a very massive system that could lens background objects and because photometry measurements can be made very accurately on them in comparison with their neighbouring galaxies. Although removing the BCG with theoretical models is quite difficult, it is still a good target to look at.

Chapter 2

Introduction to Gravitational Lensing

One of the most amazing results of Einstein's theory of general relativity, regarding the distortion of space time by massive objects is gravitational lensing. The basic principle behind gravitational lensing is that light is distorted when it travels close to the potential well (the distorion of space time) of massive objects (analogous to the effect of optical lenses). Under certain conditions the background objects can be seen in multiple images and "arcs" surrounding the lensing object, this is known as strong gravitational lensing.

Figure [] is a representation of a lensing system in which a background galaxy is lensed by a cluster of galaxies and produces multiple images as observed from Earth.
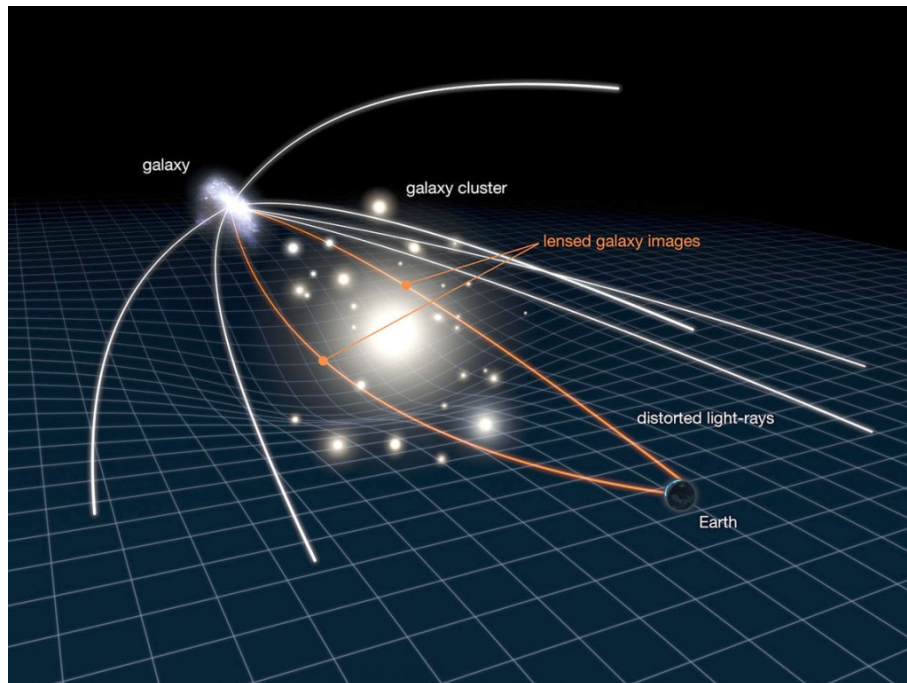
FIGURE 2.1: Nasa?

Figure [] is a composite image of a galaxy cluster taken by the HST in which many lensed objects can be seen as distorted shapes and multiple images.

FIGURE 2.2: Galaxy Cluster MACS 1206, credits to NASA Hubble Space Telescope

Quoted (need to change this):The image of galaxy cluster MACS J1206.2-0847 (or MACS 1206) is part of a broad survey with NASA Hubble Space Telescope. The distorted shapes in the cluster are distant galaxies from which the light is bent by the gravitational pull of an invisible material called dark matter within the cluster of galaxies. This cluster is an early target in a survey that will allow astronomers to construct the most detailed dark matter maps of more galaxy clusters than ever before.These maps are being used to test previous, but surprising, results that suggest that dark matter is more densely packed inside clusters than some models predict. This might mean that galaxy cluster assembly began earlier than commonly thought.

Scientists are planning to observe a total of 25 galaxy clusters under a project called CLASH (Cluster Lensing and Supernova survey with Hubble). One of the first objects observed for the new census is the galaxy cluster MACS J1206.2-0847. This conglomeration of galaxies is one of the most massive structures in the universe, and its gigantic gravitational pull causes stunning gravitational lensing. MACS 1206 lies 4 billion light-years from Earth. In addition to curving of light, gravitational lensing often produces double images of the same galaxy. In the new observation of cluster MACS J1206.2-0847, astronomers counted 47 multiple images of 12 newly identified galaxies.The era when the first clusters formed is not precisely known, but is estimated to be at least 9 billion years ago and possibly as far back as 12 billion years ago. If most of the clusters in the CLASH survey are found to have excessively high accumulations of dark matter in their central cores, then it may yield new clues to the early stages in the origin of structure in the universe.

Galaxies and clusters of galaxies that act as gravitational lenses can be approximated by single isothermal spheres. It is easy to relate an angular scaling parameter ξ_E, referred to as the Einstein radius, to the mass inside the corresponding light cone. The Einstein radius corresponds to the ring image of a point source aligned exactly on the axis of the lens.

Summary of isothermal sphere:

$$\rho(r) = \frac{\sigma^2}{2\pi G r^2} \tag{2.1}$$

$$\Sigma(\xi) = \frac{\sigma^2}{2G\xi} \tag{2.2}$$

$$\xi_E = 4\pi \left(\frac{\sigma}{c}\right)^2 \frac{D_{ds}}{D_s} \tag{2.3}$$

In reality, the density profile and lensing properties of galaxies is a bit more complicated than the assumption of a singular isothermal sphere, so we need to take into account more complex but elaborate profiles such as the NFW (Navarro, Frenk, White, 1996).

The NFW density profile is

$$\rho(r) = \frac{\delta_c \rho_c}{(r/r_s)(1 + r/r_s)^2} \tag{2.4}$$

where the characteristic over density (dimensionless quantity) is given by:

$$\delta_c = \frac{200}{3} \frac{c^3}{\ln(1+c) - c/(1+c)} \tag{2.5}$$

The mass of an NFW halo contained within a radius of r_{200} is:

$$M_{200} = M(r_{200}) = \frac{800\pi}{3} \rho_c r_{200}^3 = \frac{800\pi}{3} \frac{\bar{\rho}(z)}{\Omega(z)} r_{200}^3 \tag{2.6}$$

The concentration parameter c is strongly correlated with Hubble type, c=2.6 separating early from late-type galaxies. Those galaxies with concentration indices $c > 2.6$ are early-type galaxies reflecting the fact that the light is more concentrated towards their centres, its formal definition in terms of the virial and characteristic radius is:

$c = r_{200}/r_s$

Dutton and Maccio 2014 (in continuation of previous studies such as Muñoz Cuartas et. al. 2010), made simulations of halo masses from dwarf galaxies to galaxy clusters and find constraints on the concentration parameter for different redshifts, the relation between the concentration parameter with redshift and virial mass is shown in figure [].
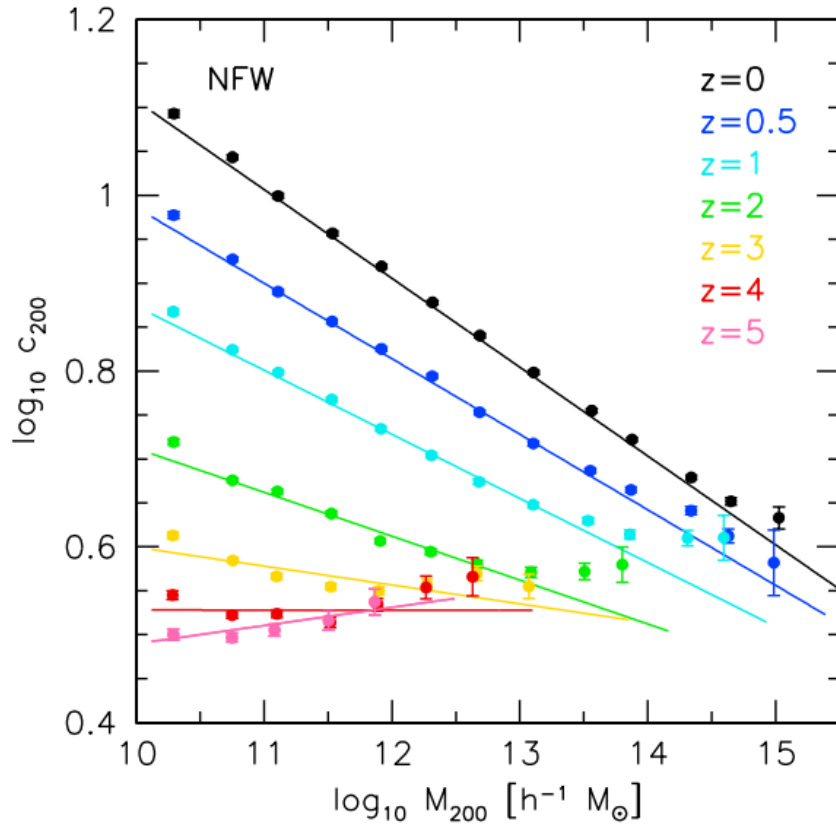
FIGURE 2.3: Evolution of the concentration mass relation, by Dutton & Maccio, 2014

The surface mass density in the NFW profile is given by:

$$\Sigma_{\text{NFW}}(x) = \begin{cases} \frac{2r_s\delta_c\rho_c}{(x^2-1)}\left[1 - \frac{2}{\sqrt{1-x^2}}\operatorname{arctanh}\sqrt{\frac{1-x}{1+x}}\right] & (x < 1) \\[2ex] \frac{2r_s\delta_c\rho_c}{3} & (x = 1) \\[2ex] \frac{2r_s\delta_c\rho_c}{(x^2-1)}\left[1 - \frac{2}{\sqrt{x^2-1}}\arctan\sqrt{\frac{x-1}{1+x}}\right] & (x > 1) \end{cases} \qquad (2.7)$$

so from the critical density:

$$\rho_c = \frac{3H^2(z)}{8\pi G} \qquad (2.8)$$

$$H(z) = H_0(1 + \Omega z)^{3/2}$$

But we are more interested in the enclosed mass which can be done by integrating the surface mass density:

$$M(R) = \int_0^R 2\pi R \Sigma(R) dR \tag{2.9}$$

The radial dependence on the shear is:

$$\gamma_{\mathrm{NFW}}(x) = \begin{cases} \frac{r_s \delta_c \rho_c}{\Sigma_c} g_<(x) & (x < 1) \\[2ex] \frac{r_s \delta_c \rho_c}{\Sigma_c} \left[\frac{10}{3} + 4 \ln \left(\frac{1}{2} \right) \right] & (x = 1) \\[2ex] \frac{r_s \delta_c \rho_c}{\Sigma_c} g_>(x) & (x > 1) \end{cases} \tag{2.10}$$

where:

$$g_<(x) = \frac{8 \operatorname{arctanh} \sqrt{\frac{1-x}{1+x}}}{x^2 \sqrt{1-x^2}} + \frac{4}{x^2} \ln \left(\frac{x}{2} \right) - \frac{2}{(x^2-1)} + \frac{4 \operatorname{arctanh} \sqrt{\frac{1-x}{1+x}}}{(x^2-1)(1-x^2)^{1/2}} \tag{2.11}$$

$$g_<(x) = \frac{8 \arctan \sqrt{\frac{x-1}{1+x}}}{x^2 \sqrt{x^2-1}} + \frac{4}{x^2} \ln \left(\frac{x}{2} \right) - \frac{2}{(x^2-1)} + \frac{4 \arctan \sqrt{\frac{x-1}{1+x}}}{(x^2-1)^{3/2}} \tag{2.12}$$

and with the critical surface mass density:

$$\Sigma_c \equiv \frac{c^2}{4\pi G} \frac{D_s}{D_d D_{ds}} \tag{2.13}$$

these equations come from the paper Wright and Brainerd 1999.

The magnification tensor is:

$$\frac{\partial \beta}{\partial \theta} = \delta_{ij} - \frac{\partial^2 \psi}{\partial \theta_i \partial \theta_j} = \begin{pmatrix} 1 - \kappa - \gamma_1 & -\gamma_2 \\ -\gamma_2 & 1 - \kappa + \gamma_1 \end{pmatrix} \tag{2.14}$$

The total magnification μ is given by the determinant of the magnification tensor:

$$\mu = \frac{1}{(1-\kappa)^2 - \gamma_1^2 - \gamma_2^2} \tag{2.15}$$

Where κ is the convergence that determines the magnification and γ_1 and γ_2 are the shear components that determine the distortion of the background objects.

Chapter 3

Scales to probe

Galaxy clusters are known to be the most massive bound structures in the Universe and dominated by their dark matter component.

The plot of the enclosed mass shows what radial scale we need to prove. One way could be through dynamics, another could be through gravitational lensing (talk about lensing). If we take different IMFs, how sensitive is the matter content to the choice of IMF?. Smaller the dark matter contribution, the smaller the overall error you make since light is easier to constraint and thus the IMF. Strong lensing measures exactly the enclosed mass so we need to know how much of its contribution we need to substract, the less we have to substract, the better for the determination of the IMF. If the effect of the IMF is very subtle in the mass vs radius plot, then we would need to know the dark matter distribution very well, but if the effect of the IMF is not very subtle, the less you need to know about the dark matter distribution. A recent study of a BCG mentions the relevance of this spatial scale, at very small radii stars dominate the lensing mass, so that lensing provides a direct probe of the stellar mass-to-light ratio, with only small corrections needed for dark matter (Russell Smith and John R. Lucey 2013)

That's why the IMF is relevant, because it allows to see how much it moves up and down. If you look at a galaxy, why is it not possible to get the mass to light ratio? This is because the dark matter is more diluted than stellar light so the mass follows light behavior is not valid and a well understood theory of the dark matter halos has to be taken into account, NFW (Navarro, Frenk & White, 1996) provided a very consistent model for dark matter halos using N-body simulations so we can relate the lensing of the halos given this NFW density profile and putting special attention in the spacial scales on which the dark matter is relevant and where it starts to be the dominant contribution of the system and thus the lensing.

The following plot shows the expected number of galaxies in the background of the lens objects in redshift bins. This results suggest that there msut be some lensed objects near the BCG.

CFHT can see objects as deep as m=23 but Hubble Space Telescope could see objects as deep as m=25 so it should be able to see many objects that have been lensed.
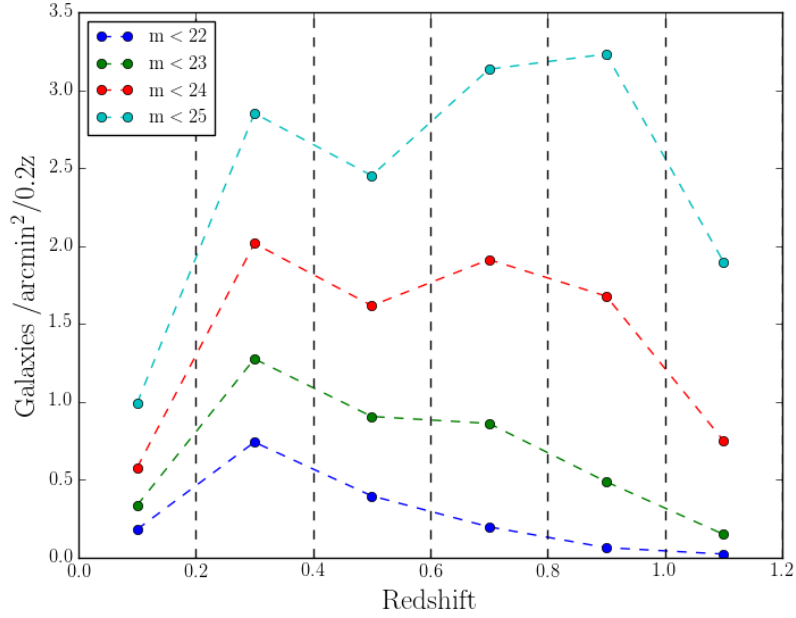
FIGURE 3.1: Galaxies per acrmin in redshift bins

Around z=0.3 is the peak of the number of galaxies so we can measure the Einstin ring for objects located at that distance and look carefully into our data to find them.

From the paper of Lokas and Mamon, for constant mass-to-light-ratio we have $\Sigma_M(R) = \Upsilon I(R)$ where $I(R) \approx 10^7$ was found by fitting the surface brightness with `GALFIT`.

The mass to light ratio is $\Upsilon \approx 4$

For A754 we take a $M_{200} = 9.8 \times 10^{15} M\odot$ (Sifon et. al. 2015)

let's take the case of ABELL1068, it's magnitude in U is 21.94, in I is 18.46, in g is 20.09, in r is 19.5, also $M_{200} = 4.3 \times 10^{14} M_{\odot}$ (van der Burg et. al 2015)

The bolometric luminosity of Abell1068 is 10^{44}erg/s that in solar luminosities is $1.9 \times 10^{12} L_{\odot}$, this gives an effective brightness of $0.962 \times 10^7 M_{\odot}/kpc^2$.

the distance to the galaxy is 591.42857 Mpc

In the case of the ABELL1068 cluster, our estimation yields a concentration parameter of 4.46.

then the concentration parameter for ABELL1068 is about 7.9 supposing a mass of the galaxy of $10^{12.5} M_\odot$

The critical density would be: 2×10^{-26} in SI units so in $M_\odot/pc^3$ it is 2.9×10^{-7}

the Hubble parameter at z=0.138 is H(z)=85.6

The characteristic radius is given by $r_{1/2} = 1.34 R_e$

For the stellar content of the cluster we can use de Vaucouleurs law for the surface brightness distribution in giant elliptical galaxies which is:

$$I(R) = I_e e^{-b\left[(R/R_e)^{1/4}-1\right]} \tag{3.1}$$

where $b = 7.67$ and I_e is the effective brightness which is basically the brightness at the effective radius R_e

Hence we have the surface mass density for both the stellar content and the NFW profile, as shown in figure [].
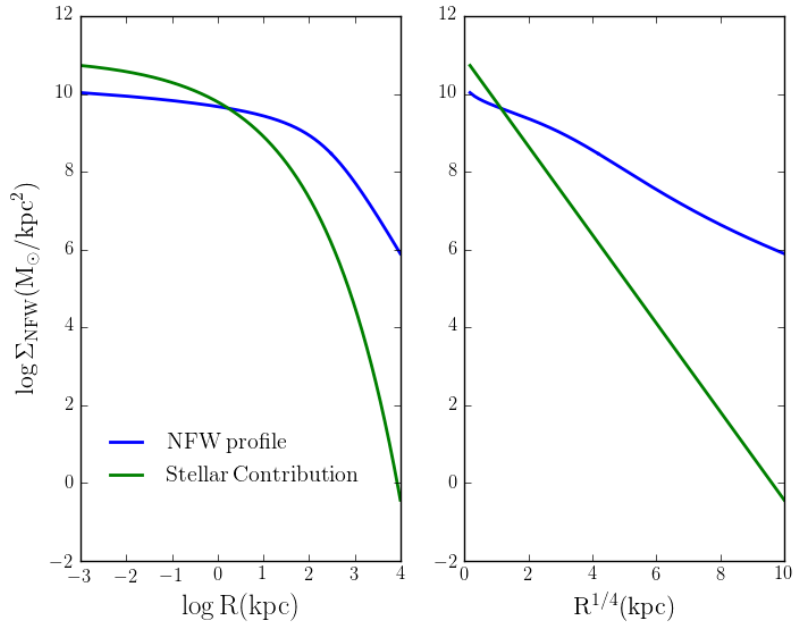

FIGURE 3.2: Surface mass density profiles in logarithmic and $R^{1/4}$ scale for the NFW profile and the stellar component.

And we can recover our luminosity by integrating the surface brightness profile accordingly:

$$L = \int_0^R 2\pi R I(R) dR \qquad (3.2)$$

The integration gives a value that is comparable to the one found using Faber-Jackson relation: $L = \Upsilon \times \sigma^4 \approx 1.2 \times 10^{12} M_\odot$

The enclosed mass profile for stellar and dark matter content is shown in figure [].
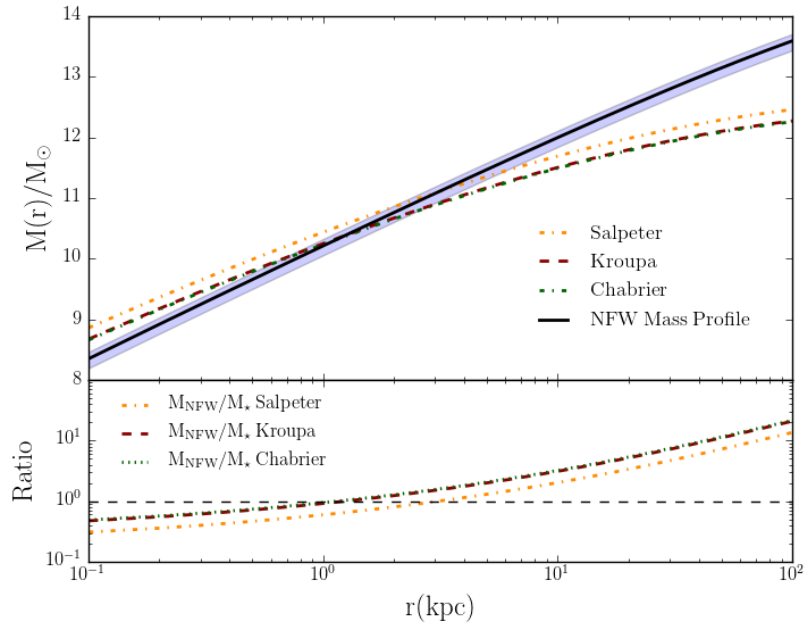
FIGURE 3.3: Enclosed mass and DM to stellar mass ratio

The value found for the mass in light is $M_\star = 2.582 \times 10^{11} M_\odot$ and the mass given by the NFW profile is $M_{\mathrm{NFW}} = 6.557 \times 10^{11} M_\odot$.

It is then usefull to study cases in which the lens system is an elliptical galaxy following its own dark matter halo and not inside the potential well of a cluster in the case of the BCG. As calculated by Sonnenfeld et. al. 2012, the encounter of the enclosed mass profiles for DM and stars for the system fdfdfds is $3kp$ which is a larger radius than the one calculated for a BCG inmerse in the halo of a low redshift cluster.
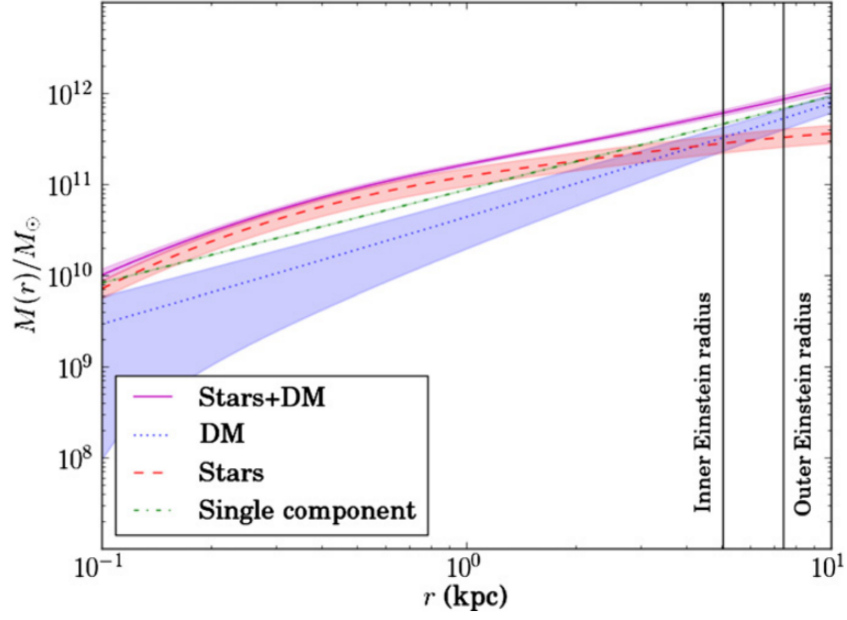
FIGURE 3.4: Mass profile for dark matter and stellar content for the lens system SDSSJ0946+1006. Sonnenfeld et. al. 2012

Now, we are interested in having an accurate estimate of the Einstein radius to constraint the model, so we make different analysis on the radial dependence on the lensing properties such as shear, reduced shear and magnification.

the plot of the shear dependence on the radius is shown in fogure [].
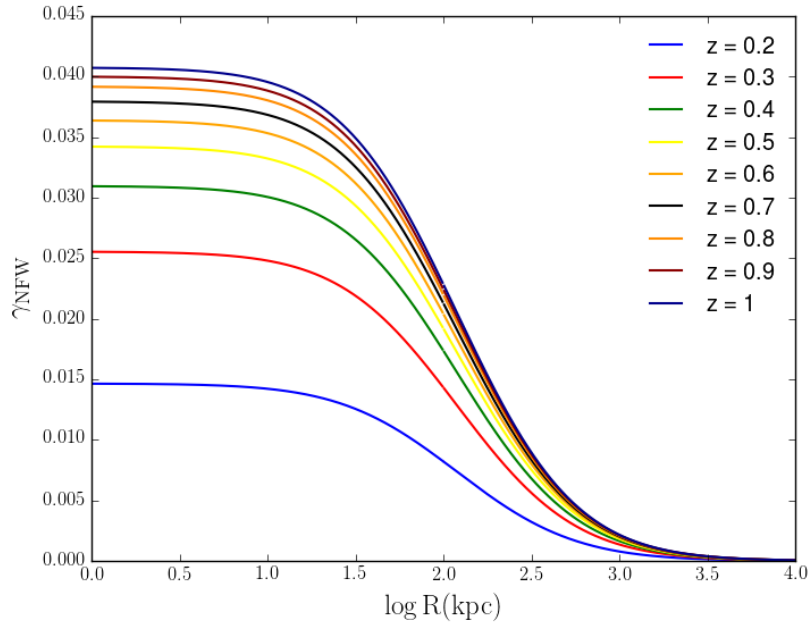
FIGURE 3.5: Shear dependence on radius for different redshift of the background galaxies
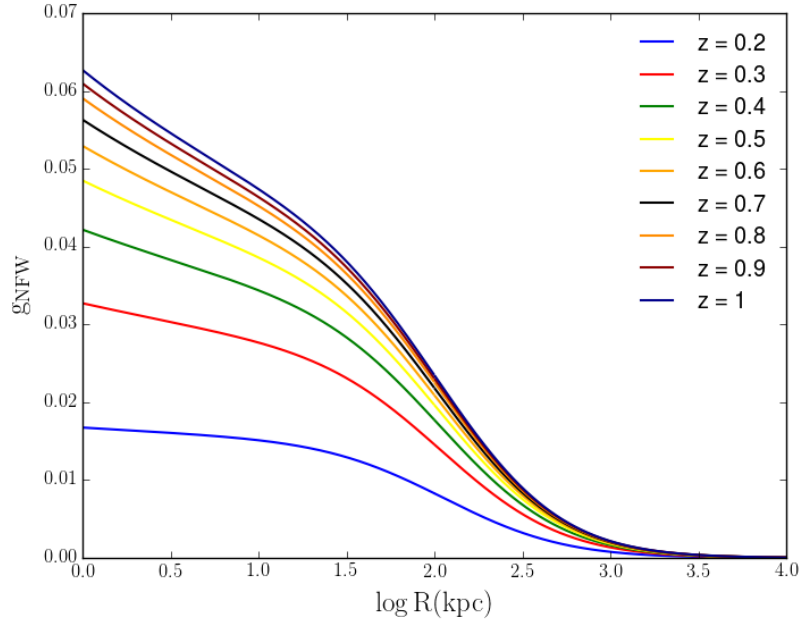
Figure [] shows the magnification.
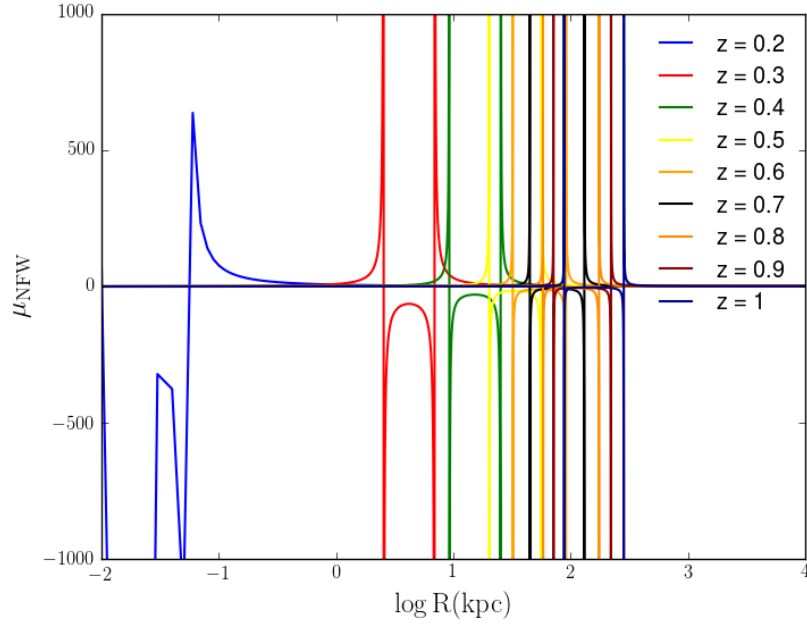
FIGURE 3.6: Magnification radial profile for various redshifts

The reduced shear is given by:

$$g = \frac{\gamma}{1 - \kappa} \tag{3.3}$$

The reduced shear for background objects at different redshifts is shown in figure [].

FIGURE 3.7: Reduced shear radial profile for different redshifts.

so we get the Einstein ring where μ is infinite or when g is 1 (k=1/2)

3.1 IMF in BCGs

Several recent studies have investigated whether the IMF systematically varies with galaxy mass, in particular among elliptical galaxies. These analyses are mostly based on two independent approaches. The first is an indirect method, where galaxy stellar masses are determined from stellar population synthesis models that actually do not resolve the IMF: the IMF is adjusted until the population-synthesis mass-to-light ratio matches independent constraints from dynamics and/or lensing. The second, direct method uses features in galaxy spectra that are particularly sensitive to the presence of, e.g., dwarf stars to determine the IMF directly from spectroscopic observations. Both approaches come to the same result: although there is significant galaxy to galaxy scatter, lower mass early-type galaxies (with dispersions $\sigma \approx 200$km/s) seem to be roughly consistent with a Milky-Way type IMF (e.g. a Kroupa or Chabrier IMF). In high-dispersion elliptical galaxies, however, stellar mass-to-light ratios are about a factor of 2 times higher than expected from a Kroupa IMF. Direct studies specifically indicate that the IMF in massive galaxies seems to be more dwarf dominated than in the Milky-Way (and can be described, e.g., by a Salpeter IMF).

Van der Vurg Thesis: *The adopted $M_\star/L$ is a major systematic uncertainty in any study and depends on the assumed IMF due to differences in the contribution of low mass stars to the total mass. We transform the results from other studies to the Chabrier IMF by subtracting 0.24 dex in mass for a Salpeter IMF, or adding 0.04 dex to the mass for a Kroupa IMF. The $M_\star/L$ depends on galaxy type, but due to the lack of multi-wavelength photometry, it is often assumed that all cluster galaxies are composed of the same stellar population. If one assumes an old stellar population (and therefore a high $M_\star/L$), the mass of the late-type galaxies (and thus the cluster as a whole) is over-estimated.* 2015
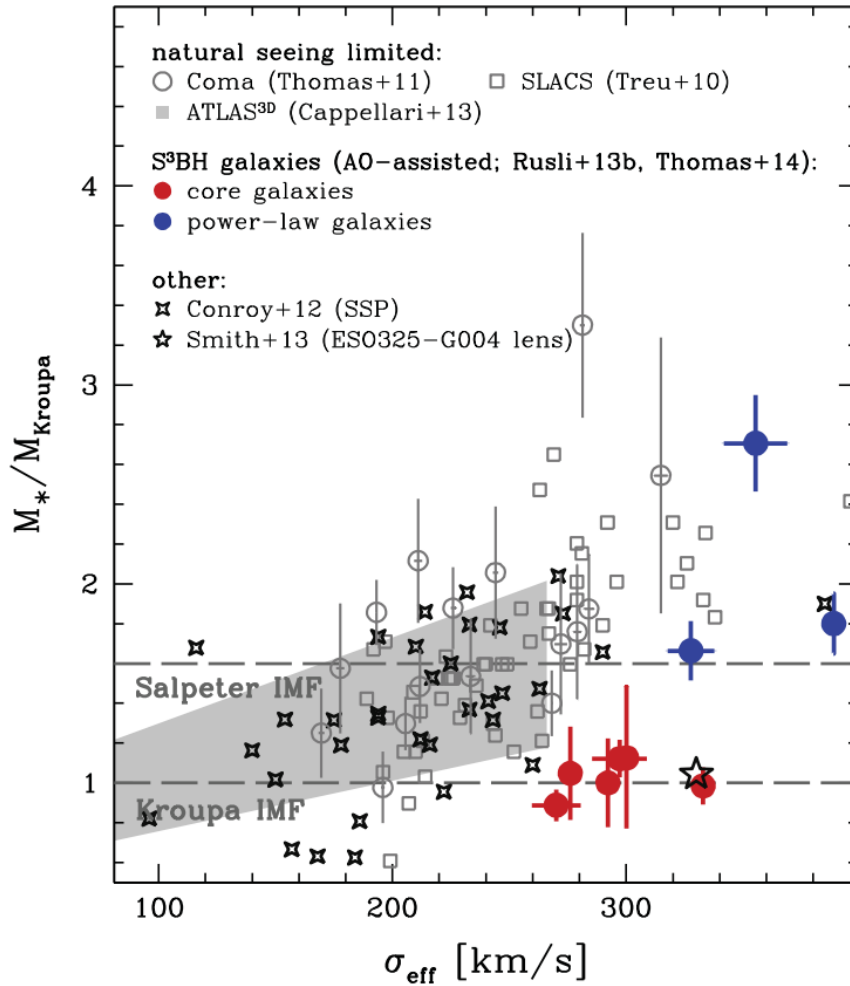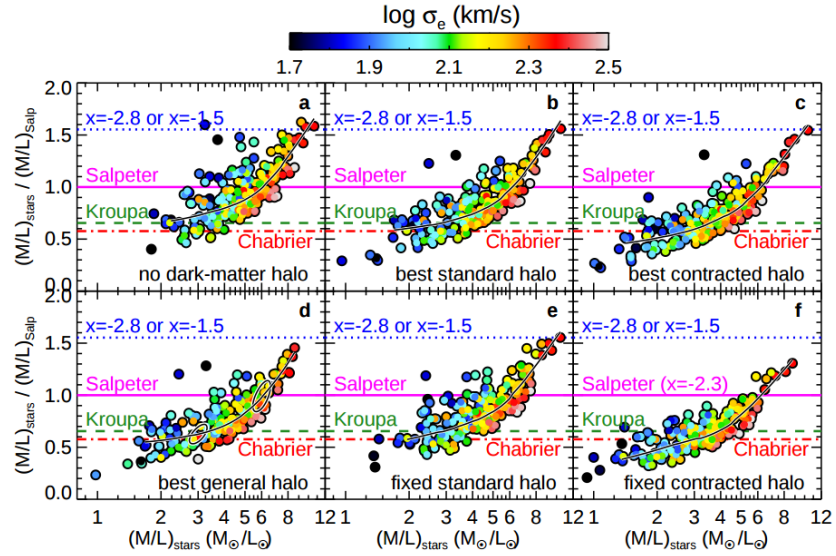

FIGURE 3.8: R

number of stars per unit mass

Kroupa, Chabrier, Salpeter,

FIGURE 3.9: The systematic variation of the IMF in early-type galaxies, Cappellari et. al. 2012.

Heavyweight

It's difficult to see how much of the faint stars contribute to the mass of the system. We only see the new bright ones

For stars, measurements of the luminosity function can be used to derive the Initial Mass Function (IMF). For galaxies, this is more difficult because Mass to light ratio (M/L) of the stellar population depends upon the star formation history of the galaxy. Bulges have heavier IMFs than disks

Several recent studies have presented evidence for "heavyweight" IMFs in giant ellipticals, with a mass-to-light-ratio twice that of a Milky Way like IMF.

Chapter 4

Data and analysis

The full description of the survey is in: D. J. Sand et. al. 2011

MegaCam wide field imager on the CFHT (Canada-France-Hawii Telescope). The cluster sample consisted of 101 clusters within the range of redshifts from 0.05 ¡ z¡ 0.55

58 clusters from the MENEACs (Multi-Epoch Nearby Cluster Survey)

The meneacs clusters represent all clusters in the BAX X-ray cluster database that are observable for the CFHT (Canada France Hawaii Telescope)

About 60 clusters, but we used only 30 for the final studies and paid special attention to 10, marked with *

G, U, I and R images

The original images have dimensions of [11000:11000] pixels but since our relevant region is the center of the cluster where the BCG is located, we cut the images with dimension of [1000,1000] for the color analysis and [4000:4000] to characterize the colors and discriminate between cluster and non-cluster members.

The INT images were multiple exposures so it was necessary to make a mosaic of them using SWARP.

4.1 Stellar populations

Galaxy clusters contain a population of stars gravitationally unbound to individual galaxies, yet still bound to the clusters overall gravitational potential, created by the stripping of stars from galaxies during interactions and mergers

Cluster	z	$\sigma(km/s)$	$d(Mpc)$	$\theta_E('')$
A1033	0.126	762	540	14.6155
A1068*	0.138	740	591.4	13.5945
A1132	0.136	727	582.9	13.1515
A119*	0.044	875	188.6	21.0798
A1413*	0.143	881	612.9	19.1569
A1650	0.084	720	360	13.6758
A1651	0.085	903	364.3	21.4876
A1795	0.062	778	265.7	16.3514
A2029*	0.077	1152	330	35.2776
A2050	0.118	854	505.7	18.5258
A2055	0.102	697	437.1	12.5642
A2064	0.108	675	462.9	11.7048
A2065*	0.073	1095	312.9	32.0110
A2069	0.116	966	497.1	23.7574
A2142*	0.091	1086	390	30.8756
A2319*	0.056	1101	240	32.9563
A2420	0.085	800	364.3	16.8653
A2440	0.091	766	390	15.3608
A2597	0.085	682	364.3	12.2569
A2627	0.126	800	540	16.1096
A2703	0.114	800	488.6	16.3307
A399	0.072	800	308.6	17.1049
A553	0.066	800	282.9	17.2155
A655*	0.127	800	544.3	16.0911
A754*	0.054	800	231.4	17.4367
A763	0.085	800	364.3	16.8653
A795	0.136	800	582.9	15.9252
A85*	0.055	800	235.7	17.4182
A961	0.124	800	531.4	16.1464
A990	0.144	800	617.1	15.7778

TABLE 4.1: Abell clusters and their redshifts as given by C. Bildfell et. al. 2012. Marked with * the chosen clusters with the most promising features

4.2 Stellar Populations

Mass-to-light ratios of early-type galaxies are of particular interest to understand the tilt of the fundamental plane. Virial relations imply that the effective surface brightness I_{eff}, the effective radius r_{eff} and the central velocity dispersion σ_0 in hot stellar systems are not independent of each other. This is revealed by the fundamental plane of early type galaxies.

The Salpeter IMF implies more low-mass stars and a higher mass-to-light ratio. In the R-band the scaling between the two cases is $\Upsilon_{\mathrm{Salp}} \approx 1.56 \Upsilon_{\mathrm{Krou}}$

A Koupra IMF finds a value of around 4 for the mass to light ratio Υ. (R. J. Smith 2014). Massive galaxies - Salpeter is a good IMF. Salpeter is heavier than Kroupa. Salpeter mass function is $n(M) \propto M^{-2.3}$

Large M/L ratios could arise either from an excess of faint dwarf stars in a "bottom heavy" IMF, or from an excess of dark remnants in a "top heavy" IMF" (Russell J. Smith and John R. Lucey 2013).

4.3 Sextractor

Segmentation image that will be used as a mask image (bad pixels) for `GALFIT`

We need to discriminate between field stars and the galaxies of the cluster so in order to do this, we used some of the parameters found by `SEXTRACTOR` that allow us to constraint the fitted data. These are class-star, flux_radius, and FWHM (full wicth half maximum). Class-star uses the neural network star/galaxy of `SEXTRACTOR` that will give values close to 1 for stars and 0 for galaxies. flux_radius, and FWHM are closely related to each other and give the radius which contains half of the light of the object so it will be small for stars and bigger for extended objects.

In order to extract the same objects and make the segmentation masks for the desired objects in the different filters, we used `SEXTRACTOR` on dual mode
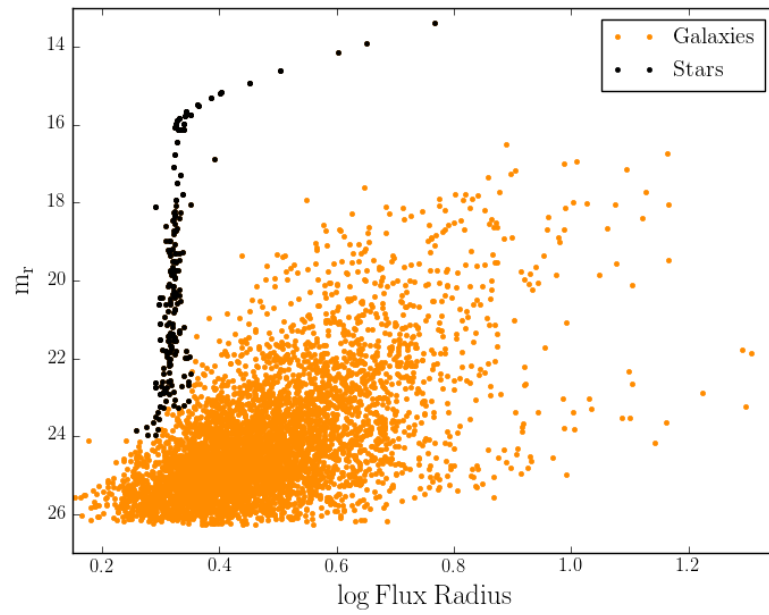
Color magnitude diagram for A1068

we used a zero point magnitude of 30
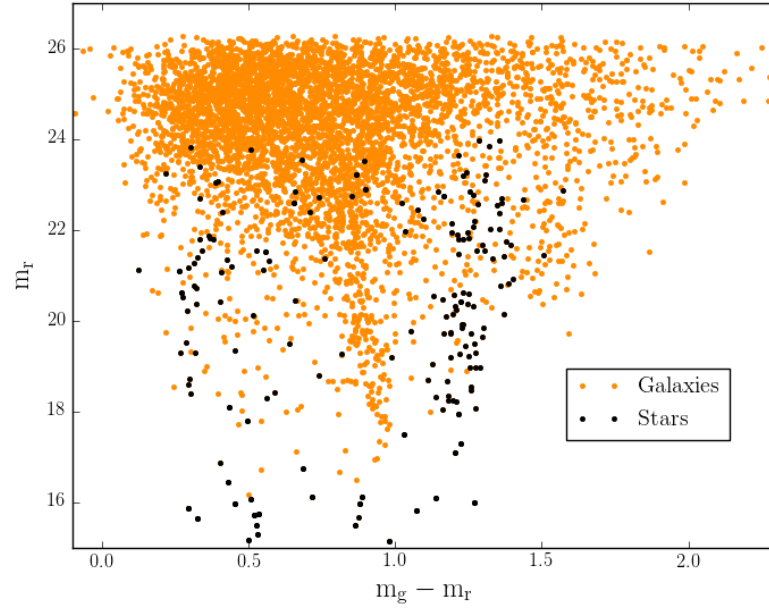
FIGURE 4.1: Color Magnitude diagram of A1068 with the differentiation of stars from galaxies

Mag vs flux rad to discriminate

FIGURE 4.2: Magnitude vs Flux radius of A1068 to identify the galaxies using the criteria of their flux distribution

4.4 Galfit

`GALFIT` (Peng et. al 2002) fits two dimensional profiles so it is a useful tool to remove the light from the BCG and allow us to observe background objects

Fit Sersic profiles with n=4 which is de Vaucouleurs profile.

A first run gives us a rough idea of the true position of the center of the BCG so we can set this values in a second run for each cluster. We needed to combine different Sersic parameters, as well as Fourier and bending modes for some of the BCGs.

We use the segmentation masks given by `SEXTRACTOR` to mask bright objects in the fitting of the BCG

the fitting of many objects (not only the BCG)

the best results were given when we masked the innermost region of the BCG so the fitting will put more weight in the rest of the profile, thus reducing most of the light that hides the background objects.

we have to take into account the magnification bias

The parameters C0, B1, B2, F1, F2, etc. listed below are hidden from the user unless he/she explicitly requests them. These can be tagged on to the end of any previous components except, of course, the PSF and the sky – although `GALFIT` won't bar you from doing so, and will just ignore them. Note that a Fourier or Bending mode amplitude of exactly 0 will cause `GALFIT` to crash because the derivative image `GALFIT` computes internally will be entirely 0. If a Fourier or Bending amplitude is set to 0 initially `GALFIT` will reset it to a value of 0.01. To prevent `GALFIT` from doing so, one can set it to any other value.

Bending modes B1) 0.07 1 Bending mode 1 (shear) B2) 0.01 1 Bending mode 2 (banana shape) B3) 0.03 1 Bending mode 3 (S-shape)

Azimuthal fourier modes F1) 0.07 30.1 1 1 Az. Fourier mode 1, amplitude and phase angle F2) 0.01 10.5 1 1 Az. Fourier mode 2, amplitude and phase angle F6) 0.03 10.5 1 1 Az. Fourier mode 6, amplitude and phase angle F10) 0.08 20.5 1 1 Az. Fourier mode 10, amplitude and phase angle F20) 0.01 23.5 1 1 Az. Fourier mode 20, amplitude and phase angle

Traditional Diskyness/Boxyness parameter c C0) 0.1 0 traditional diskyness(-)/boxyness(+)

The masks:
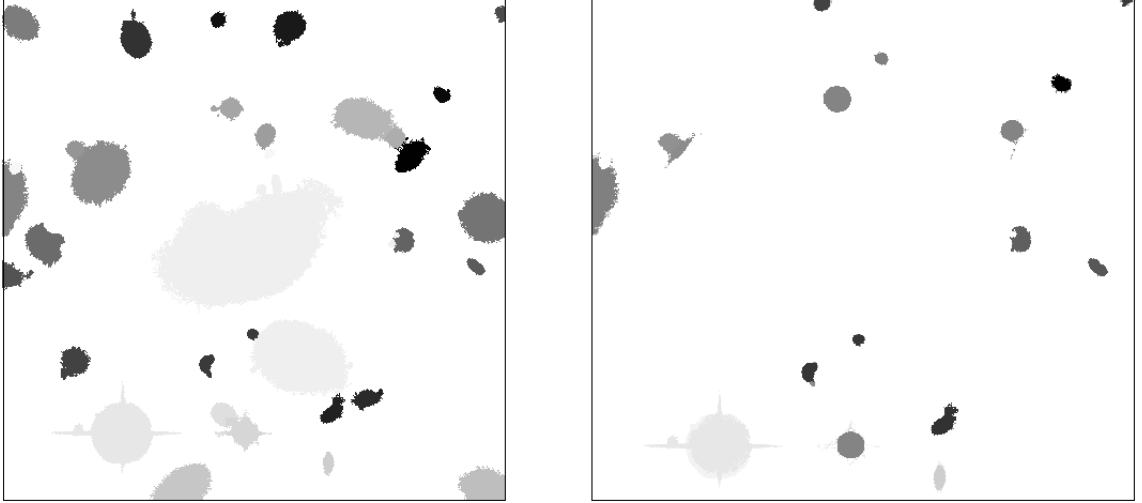
FIGURE 4.3: Segmentation images produced by SEXTRACTOR and used as mask files for the galfit extraction. Left panel is the original mask with all the bright objects. Right panel is the mask after the substraction of the regions surrounding the cluster galaxies to be fitted with GALFIT.

The colors are inverted for an easier visualization of the image. The fainter regions are actually the most luminous objects because GALFIT assigns increasing numbers starting from the brightest one, that is the BCG in this case

The original image, the fitted models and the output are presented here:
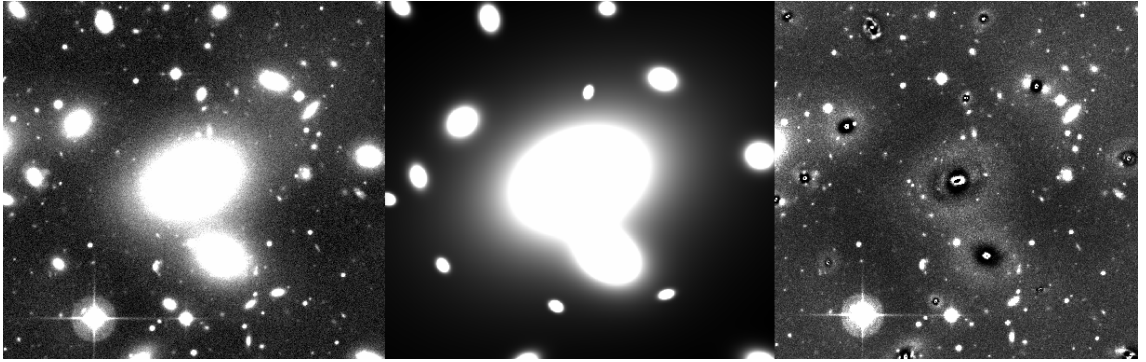

FIGURE 4.4: Galfit procedures. Left: Original image in zscale with the clear BCG expanding across a significant region of the central area. Middle: The models fitted by GALFIT for all the selected cluster galaxies. Right: Residual image after the substraction of the model galaxies.

4.5   Color images

We use IRAF to make the color images using our g,r,u,i bands

Here we take an isothermal sphere to model the Einstein ring in a distance of background objects of z=1

We made a color image of the original center of the cluster without subtracting the BCG in order to differentiate between cluster members from background galaxies and field stars. This allows us to fit only the cluster galaxies.
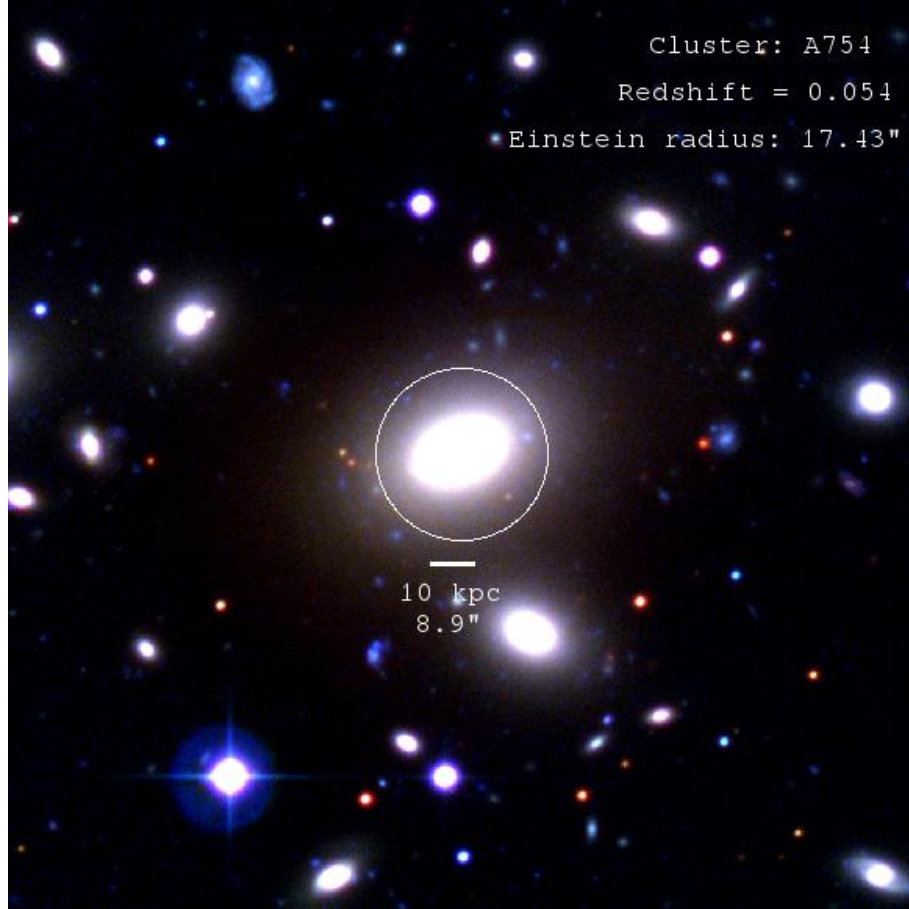
FIGURE 4.5: Color image of A754 cluster (filters i,g,u) with its Einstein radius calculated for an isothermal sphere of a background object at $z = 1$.

After choosing the galaxies that belong to the cluster by comparing their relative colors, we subtracted them using `GALFIT` and made the color image again changing the scaling values with the task `CONVERT` of `IRAF` so that we see can see the color contrast to search for good candidates of lensed objects. By looking at this reduced color image, we have another visual constraint to choose the clusters in which it would be worth to do photometric redshifts and search for objects with the same redshift in different locations around the very center of the BCG (object that has suffered strong lensing).
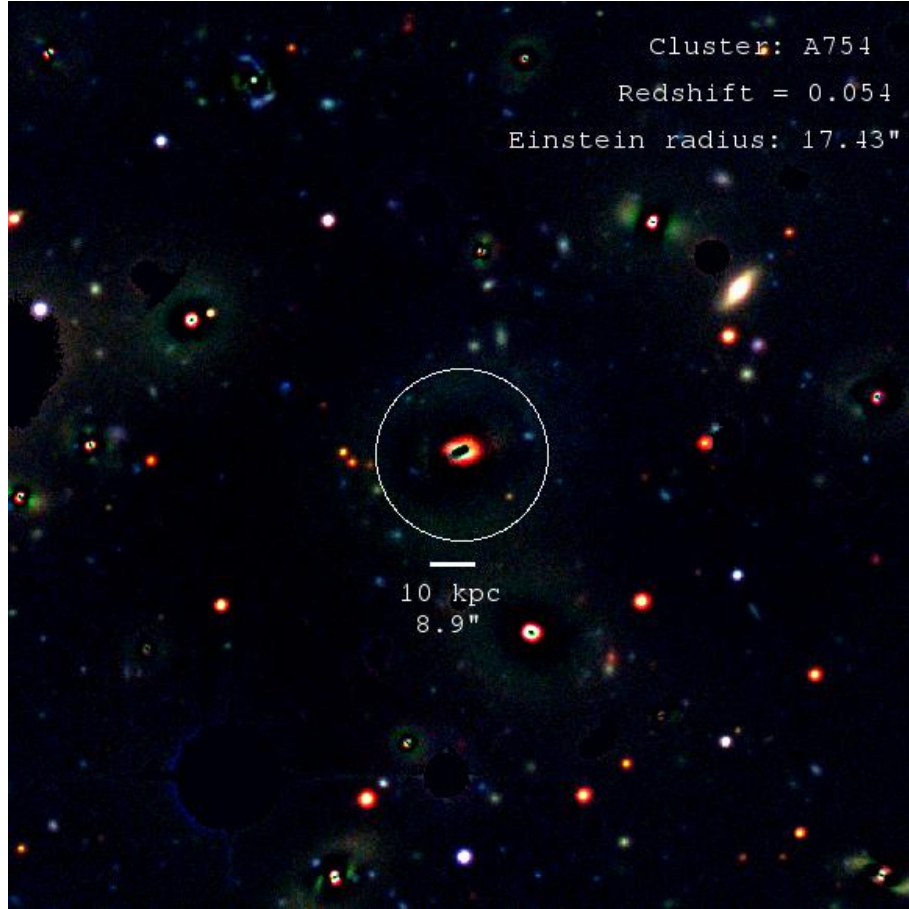
FIGURE 4.6: Color image of A754 cluster (filters i,g,u) after the substraction of the bright cluster galaxies.

Because we have 4 bands we were able to make different color images to see the contrast and make combinations that would allow us to see better the very red and very blue objects, in the following figure we have the g-r, i-r-g and i-g-u color images for three clusters.
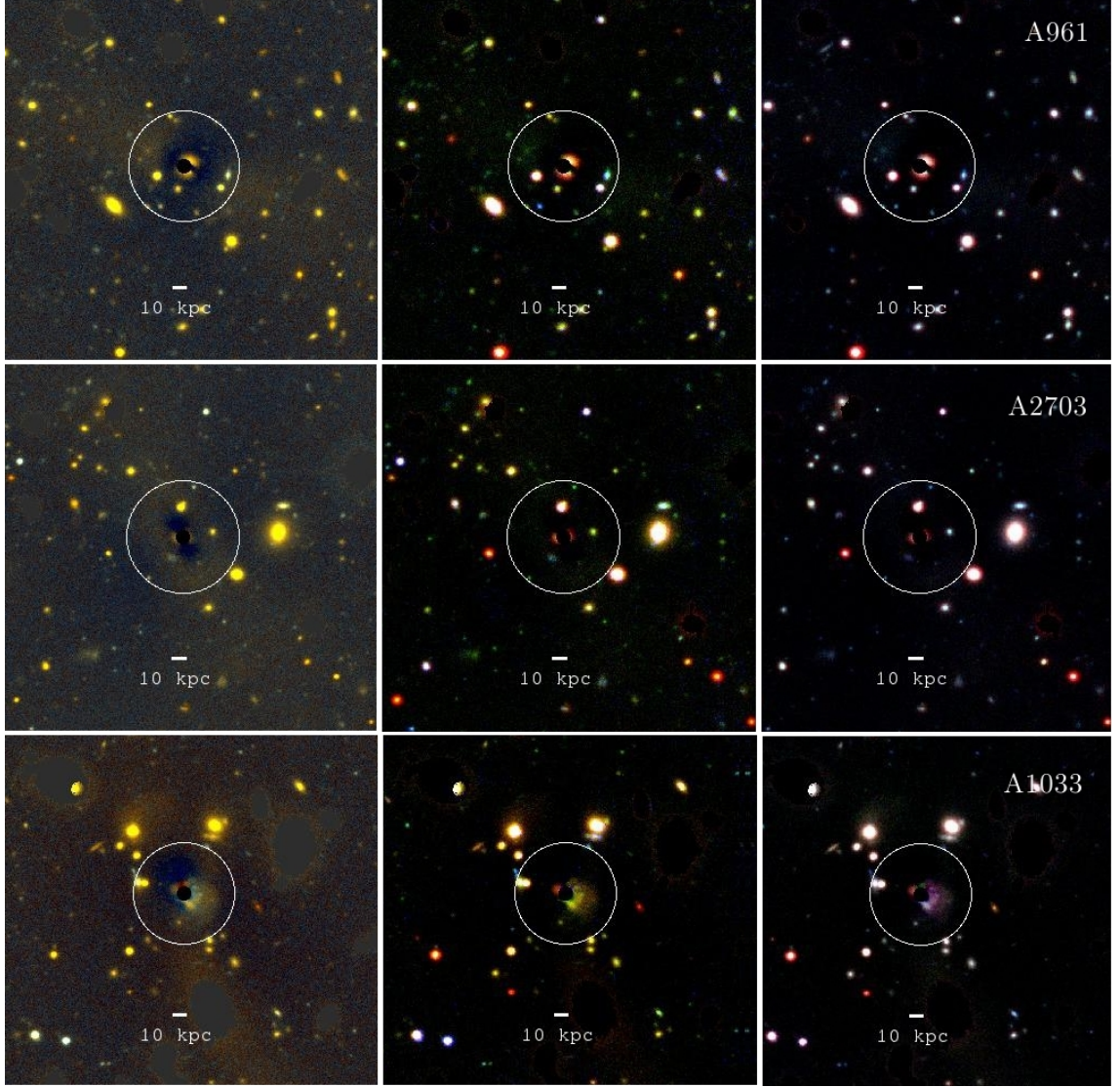
FIGURE 4.7: Different color images for different combination of the g,r,u,i filters for the clusters A961, A2703, A1033. Left column for the images constructed only with the g and r filter, central column for i,g,r and right column for i,g,u.

4.6   Photometric Redshifts

We use the *COSMOS2015* (Laigle et. al 2016.) catalogue that contains photometric redshift of over half million galaxies in multiple bands to put another constraint in our study.

We use the matched catalogue for CFHT by ⸺ and use the r-band. Our limiting magnitude is 23 in that band so we estimate the number of galaxies per redshift bin that we would expect to see in our sample with that limiting magnitude.

This sets an interesting constraint on what to expect in the inner region of the BCG and give us more information about where to search for good candidates.

The limiting magnitude is found using `SEXTRACTOR` that gives a good confidence on the detection of objects.

The COSMOS catalogue contains one square arcmin so we use this result to see what order we should spect from background objects.

To measure the photometric redshift of the galaxies (after filtering out the stars) in the inner region of the cluster after the subtraction of the BCG, we use the photometric redshift code EAZY (Brammer et. al 2008) which uses an extensive collection of spectral energy distributions for galaxies in the range $0 < z < 4$. Fortunately, the code includes library from CFHT in the I and U bands but doesn't have the filters in the G and R bands so I used the SUBARU survey filter information to be able to compute the photometric redshifts using four bands.

citation of EAZY "Brammer, van Dokkum and Coppi, 2008"

Chapter 5

Conclusions

We don't expect too many sources in our sample data.

Bibliography

[1] John. Smith, Russell & Lucey. A giant elliptical galaxy with a lightweight initial mass function. *MNRAS*, 000:1–14, 2013.

[2] Brewer et. al. The swells survey. vi. hierarchical inference of the initial mass functions of bulges and discs. *MNRAS*, 000:1–13, 2012.

[3] Navarro. Frenk & White. The structure of cold dark matter halos. *The Astrophysical Journal*, 462:563–575, 1996.

[4] Tommaso Treu. Strong lensing by galaxies. *Annual Review of Astronomy ans Astrophysics*, 48:87–125, 2010.

[5] Matthew R. George et. al. Galaxies in x-ray groups. ii. a weak lensing study of halo centering. *The Astrophysical Journal*, 757:2–18, 2012.

[6] D. Harvey et. al. A detection of wobbling brightest cluster galaxies within massive galaxy clusters. *MNRAS*, 000:1–9, 2017.

[7] J. C. Mu noz Cuartas et. al. The redshift evolution of λcdm halo parameters: concentration, spin and shape. *MNRAS*, 000:1–11, 2010.

[8] A. Sonnenfeld et. al. Evidence of dark matter contraction and a salpeter initial mass function in a massive early-type galaxy. *The Astrophysical Journal*, 752:163–180, 2012.

[9] R. F. J. Van der Burg et. al. Evidence for the inside-out growth of the stellar mass distribution in galaxy clusters since $z \approx 1$. *preprint arXiv:1412.2137v2*, 2015.

[10] Cappellari et. al. Systematic variation of the stellar initial mass function in early-type galaxies. *Nature*, 484:485–488, 2012.

[11] D. J. Sand et. al. Intracluster supernovae in the multi-epoch nearby cluster survey. *The Astrophysical Journal*, 729:142–155, 2011.

[12] C. Bildfell et. al. Evolution of the red sequence giant to dwarf ratio in galaxy clusters out to $z \approx 0.5$. *MNRAS*, 425:204–221, 2012.

[13] Russell. Smith. Variations in the initial mass function in early-type galaxies: a critical comparison between dynamical and spectroscopic results. *MNRAS*, 443: L69–L73, 2014.

[14] Peng et. al. Detailed structural decomposition of galaxy images. *The Astronomical Journal*, 124:266–293, 2002.

[15] Laigle et. al. The cosmos2015 catalog: Exploring the 1¡z¡6 universe with half a million galaxies. *The Astrophysical Journal*, 224(2), 2016.

[16] van Dokkum Brammer and Coppi. Eazy: A fast, public photometric redshift code. *ApJ*, 686(1503), 2008.